ChemPubSoc Europe

DOI: 10.1002/cctc.201501256

CHEMCATCHEM Full Papers

Nanocomposites of Platinum/Metal–Organic Frameworks Coated with Metal–Organic Frameworks with Remarkably Enhanced Chemoselectivity for Cinnamaldehyde Hydrogenation

Hongli Liu, Lina Chang, Liyu Chen, and Yingwei Li*[a]

The encapsulation of metal nanoparticles (MNPs) within metal–organic frameworks (MOFs) to form core–shell structural nanocomposites is one of the most promising methods to enhance the durability and selectivity of MOF-supported metal catalysts. However, it is still a challenge to fully encapsulate tiny MNPs inside MOFs. Herein, we report a facile and general strategy to coat MOFs on the surface of Pt/MOFs by direct homoepitaxial growth. The obtained Pt/MOFs@MOFs nanocomposites retained the intrinsic properties (e.g., crystalline structure, pore texture, and surface area) of Pt/MOFs. Strikingly, the MOF-coated materials exhibited a significantly enhanced chemoselectivity compared to the uncoated materials, for example, in the hydrogenation of cinnamaldehyde, the selectivity to cinnamyl alcohol through C=O hydrogenation was improved from 55 to 96% at complete conversions of cinnamaldehyde. Moreover, Pt/MOFs@MOFs can be recycled without any remarkable loss in both activity and selectivity. The enhanced catalytic selectivity and stability of MNPs/MOFs could be related to the synergetic effects of the electron donation and nanoconfinement offered by the surrounding MOF networks.

Introduction

Supported metal nanoparticles (MNPs), among the most important classes of heterogeneous catalysts, are widely used in industrial applications because of their facile recovery, but unfortunately they generally exhibit lower selectivities to the desired products compared to homogeneous catalysts.[1] Consequently, great efforts have been devoted to the development of new strategies to enhance the reaction selectivity of MNPs.[2]

Among the already developed strategies, a promising approach is to encapsulate MNPs within appropriate porous materials. Steric restrictions might be imposed on the confined MNPs, and their electronic configuration would be modified by the surrounding porous shell, which would create a different microenvironment around the MNPs compared with that of the nonencapsulated analogues. This microenvironment can not only protect the MNPs from leaching and aggregation/sintering during reactions but also, importantly, may induce improved selectivity toward target molecules because of the electronic interactions and steric restrictions as well as the orientation of the reactive groups. Mesoporous silicas, which possess good stability and high surface areas and pore volumes, are currently utilized widely as shells for MNPs.[2a–d,3] However, the amorphous structure of silica and its inherent shortcomings make it difficult to achieve satisfactory confinement effects (in particular for electronic interactions) to improve the chemoselectivity. Therefore, the exploration of new types of shell materials to enable better confinement effects to obtain an optimized catalytic performance is imperative.

Metal–organic frameworks (MOFs), which are emerging as a particular class of hybrid porous materials with many exciting characteristics,[4] might open new opportunities to achieve confinement. In addition to high specific surface areas and tunable pore sizes and volumes, MOFs possess abundant interconnected 3D cavities accessible through small pore windows.[5] This characteristic could simultaneously prevent the encapsulated MNPs from escaping from cavities or agglomerating and guarantee the easy diffusion of the reactants. Interestingly, MOFs constructed by metal nodes and aryl (hetero) linkers can certainly establish charge transfer interactions by coordination or π–π interactions, which may offer an additional electron donation effect to the encapsulated MNPs as compared to traditional porous materials such as silicas.[6] The combination of electron donation and steric restriction effects would enable MOFs to be efficient shell materials for the confinement of MNPs in terms of stability and selectivity.

Consequently, many endeavors have been devoted to the development of effective approaches to introduce MNPs into MOFs.[5a,b,6,7] Currently, the most widely adopted strategy is based on the incorporation of metal precursors as guests and followed by reduction or decomposition of the embedded precursors to form MNPs/MOFs.[5a,b,6a,7d–j] However, with these synthetic methods it is extremely difficult to encapsulate MNPs

[a] Dr. H. Liu, L. Chang, L. Chen, Prof. Y. Li
School of Chemistry and Chemical Engineering
Key Lab for Fuel Cell Technology of Guangdong Province
South China University of Technology
Guangzhou 510640 (P.R. China)
E-mail: liyw@scut.edu.cn

Supporting Information for this article is available on the WWW under http://dx.doi.org/10.1002/cctc.201501256.

fully inside MOFs because of the diffusion resistance between the external and internal MOF surfaces, which results in a lot of MNPs distributed undesirably on the external surface of the MOF crystals. Such MNPs outside the MOF lack the beneficial microenvironment offered by the MOF networks, which would make the catalyst system suffer from poor catalytic selectivity. To enhance the chemoselectivity of the MNPs/MOFs, it could be feasible to coat the MNPs/MOFs fully with MOFs to obtain MNPs/MOFs@MOFs nanocomposites.

Herein, we report a facile and general synthetic strategy to obtain designable MNPs/MOFs@MOFs nanocomposites by the direct homoepitaxial growth of a MOF shell on the surface of MNPs/MOFs (Scheme 1). To enable a perfect lattice match, the

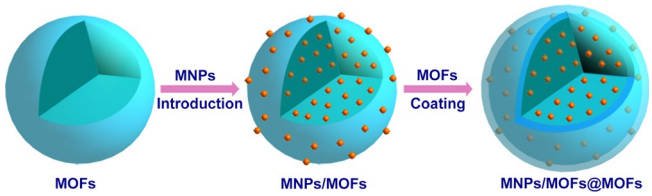

Scheme 1. Illustration of the preparation of MNPs/MOFs@MOFs nanocomposites.

same MOF is selected for the shell as that in the core to support the MNPs. Such a lattice match ensures pore connections at the interface, which may facilitate the diffusion and accessibility of reactants to the active MNPs without deteriorating the intrinsic properties of MNPs/MOFs. To demonstrate the universality of the present approach, two representative MOFs, MIL-100(Fe) and NH_2-MIL-101(Al), are investigated here. Significantly, the thickness of the outer MOF shell can be tuned in the composites, which exhibit a remarkably enhanced chemoselectivity in the hydrogenation of cinnamaldehyde. Remarkably, the selectivity to cinnamyl alcohol through C=O hydrogenation is improved from 55 to 96% at a complete conversion of cinnamaldehyde over the MNPs/MOFs@MOFs.

Results and Discussion

Initially, one of the representative mesoporous MOFs, Fe^{III}-based MIL-100 ($Fe_3O(H_2O)_2F{\cdot}[C_6H_3(CO_2)]_3{\cdot}H_2O$) with two types of large pores (25 and 29 Å) accessible through microporous windows (≈5.5 and 8.6 Å) and a high specific surface area as well as excellent stability,[8] was selected as a host matrix to incorporate Pt nanoparticles (NPs) by a simple colloidal deposition method.[6c] Given the lattice match, the resultant Pt/MIL-100 was used subsequently as the core for the epitaxial growth of an outer MIL-100 shell to produce a fully encapsulated Pt material (denoted as Pt/MIL-100@MIL-100) through a stepwise liquid-phase epitaxy method without any surface modification. The thickness of the outer MIL-100 shell can be controlled effectively by altering the number of assembly cycles.

Powder X-ray diffraction (PXRD) patterns (Figure 1) revealed no apparent loss of crystallinity upon the incorporation of Pt on MIL-100, which implies that the addition of Pt did not

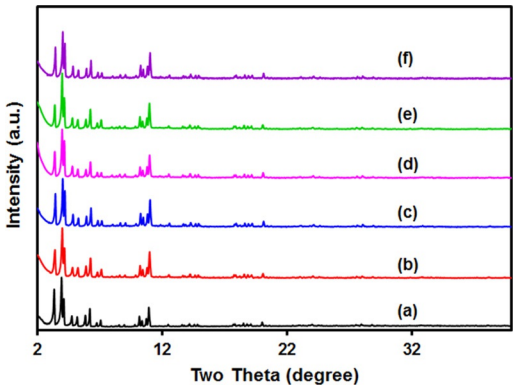

Figure 1. PXRD patterns of a) MIL-100(Fe), b) Pt/MIL-100(Fe), Pt/MIL-100(Fe)@MIL-100(Fe) prepared by c) two, d) four, and e) six assembly cycles, and f) Pt/MIL-100(Fe)@MIL-100(Fe) prepared by four assembly cycles after the catalytic reaction.

affect the framework structure of MIL-100. The PXRD patterns of the Pt/MIL-100@MIL-100 nanocomposites with different shell thickness were identical to that of the parent MIL-100, which suggests a successful epitaxial growth of the outer MIL-100 shell with the crystallographic direction of the Pt/MIL-100 core. Moreover, it is difficult for us to observe the XRD patterns of Pt, which could presumably be related to the low Pt content and the small particle size in these materials.

The specific surface areas and porosities of the samples were determined by N_2 physisorption at 77 K. All the samples displayed similar isotherms with secondary uptakes at P/P_0 ~ 0.1 and ~0.2 (Figure 2), which suggests the presence of two

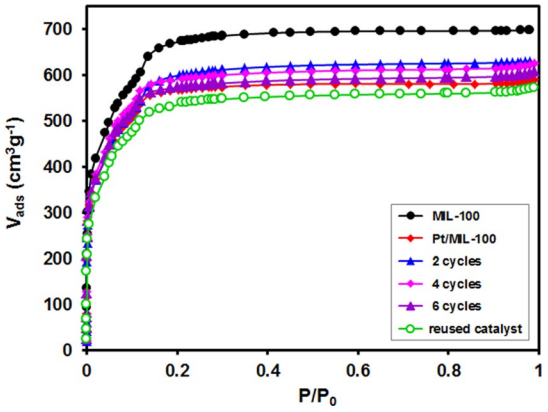

Figure 2. N_2 adsorption isotherms of MIL-100(Fe), Pt/MIL-100(Fe), and Pt/MIL-100(Fe)@MIL-100(Fe) prepared by different numbers of assembly cycles.

types of microporous windows. The BET surface area and total pore volume of MIL-100 were calculated to be 2334 $m^2 g^{-1}$ and 0.98 $cm^3 g^{-1}$, respectively. Compared to parent MIL-100, Pt/MIL-100 showed a decreased BET surface area and pore volume, mainly because of the blockage of the cavities of MIL-100 by the highly dispersed Pt NPs. After the coating of MIL-100, the N_2 adsorption amounts for the formed Pt/MIL-100@MIL-100 composites increased slightly with up to six assembly cycles, probably because of the contribution of the porous MIL-100 shell.

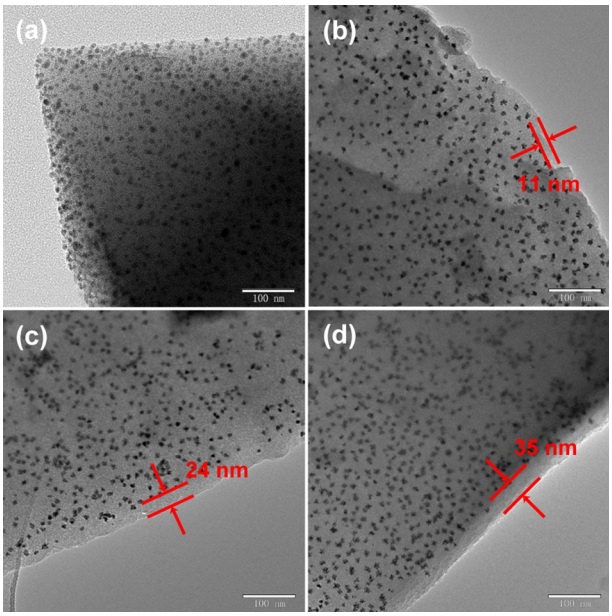

Figure 3. TEM images of a) Pt/MIL-100 and Pt/MIL-100@MIL-100 prepared by b) two, c) four, and d) six assembly cycles. Scale bars: 100 nm.

The morphology and structure of the Pt/MIL-100@MIL-100 samples were investigated by TEM. The as-prepared Pt/MIL-100 exhibited a uniform distribution of Pt NPs in the MIL-100 framework with a mean size of 3.0 nm (Figure 3 a). Some Pt particles could be observed bulging out from the MOF edges (Figure 3 a), which suggests that some of the Pt nanoparticles were doped on the outer surface of the MOF. After it was coated with MIL-100, the surface of Pt/MIL-100 was well covered with a MIL-100 shell layer and clearly exhibited a core–shell structure (Figure 3 b–d, Figure S1). The average thickness of the MIL-100 shell was ≈11, 24, and 35 nm for Pt/MIL-100@MIL-100 with two, four, and six assembly cycles, respectively. This result demonstrated that the thickness of the MIL-100 shell could be controlled effectively by varying the assembly cycle numbers. Moreover, the coating of the MIL-100 shell did not affect the distribution and size of Pt NPs in the Pt/MIL-100 significantly.

The XPS spectra of the Pt/MIL-100 and Pt/MIL-100@MIL-100 with four assembly cycles are shown in Figure 4. The binding energies of the Pt 4f 7/2 and Pt 4f 5/2 peaks for Pt/MIL-100 were observed at ≈71.3 and 74.8 eV, respectively, typical of metallic Pt, which suggests that the Pt species were mostly in the reduced state on Pt/MIL-100. After the coating with MIL-100, the Pt 4f peaks for Pt/MIL-100@MIL-100 were shifted to lower binding energies by approximately 0.2 eV compared to that of Pt/MIL-100. Such shifts may be attributed to electron donation to the encapsulated Pt NPs from the surrounding MOF networks.[6]

The selective hydrogenation of α,β-unsaturated aldehydes to their corresponding unsaturated alcohols is an important process in the industrial synthesis of fine chemicals, particularly of pharmaceuticals, perfumes, and cosmetics.[9] This is also considered as one of the most extensively investigated model reactions to verify the chemoselectivity of a catalyst because of its two distinct competing sites for hydrogenation: a C=O bond and a conjugated C=C group,[9c,d] which generally leads to a complex reaction network that involves a parallel and consecutive reduction at different functional groups (Scheme 2).

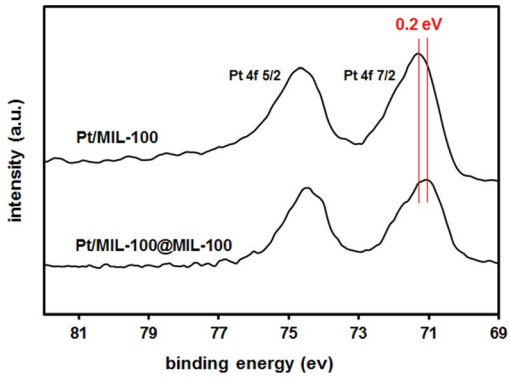

Figure 4. Pt 4f XPS spectra of Pt/MIL-100 and Pt/MIL-100@MIL-100 prepared by four assembly cycles.

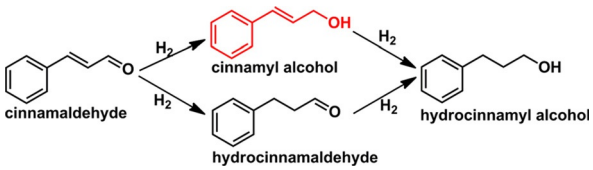

Scheme 2. Reaction network of cinnamaldehyde hydrogenation.

One product of this reaction, the unsaturated alcohol through only C=O bond hydrogenation, is more valuable industrially compared to the other products. However, it is quite difficult to achieve a high selectivity to the unsaturated alcohol product at a high conversion because the hydrogenation of the C=C bond is more thermodynamically favorable than C=O hydrogenation.[10] Thus, the development of highly chemoselective and active catalysts for the selective hydrogenation of unsaturated aldehydes to unsaturated alcohols under mild conditions is challenging but of great importance.

Here, cinnamaldehyde, a representative α,β-unsaturated aldehyde, was chosen as a model substrate to investigate the effect of the MOF coating on the chemoselectivity of Pt/MOF materials. Pt/MIL-100 provided only 55% selectivity to the desired cinnamyl alcohol (COL) at >99% cinnamaldehyde conversion within 2 h under the investigated conditions (Figure 5). To investigate the effect of residual polyvinylpyrrolidone (PVP) on the reactivity of Pt NPs, Pt/MIL-100 was heated at 220 °C for 2 h under N_2. The reaction results demonstrated that the treated Pt/MIL-100 showed negligible changes in both activity and selectivity compared to the untreated Pt/MIL-100 (Table S2), which implies that there only traces of PVP molecules remained in the material after the washing procedure that did not affect the reactivity significantly.

If Pt/MIL-100@MIL-100 prepared by two assembly cycles was employed, the selectivity to cinnamyl alcohol was enhanced to

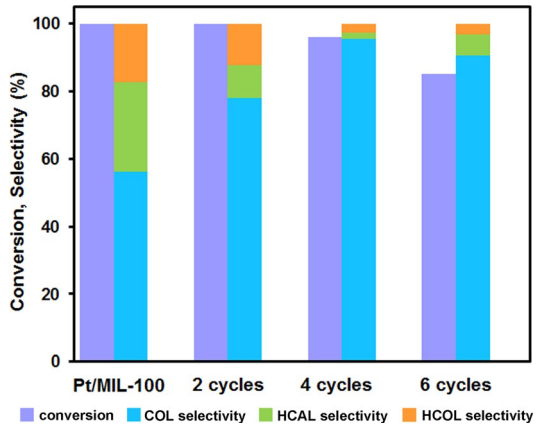

Figure 5. Catalytic results of the hydrogenation of cinnamaldehyde. Reaction conditions: cinnamaldehyde (0.5 mmol), catalyst (Pt 0.2 mol%), isopropyl alcohol (5 mL), 25 °C, 1 atm H_2.

78% at a complete conversion of cinnamaldehyde in 3 h. Pt/MIL-100@MIL-100 prepared by four and six assembly cycles also worked well in the hydrogenation reaction and displayed a 95% cinnamaldehyde conversion with 96% selectivity to cinnamyl alcohol in 4 h for the catalyst prepared by four assembly cycles and 85% conversion with 90% selectivity in 5 h for the material prepared by six assembly cycles. The above results showed that the MIL-100-coated Pt/MIL-100 materials all exhibited a higher selectivity to cinnamyl alcohol than the uncoated Pt/MIL-100 catalyst. To account for the increased Fe content after MIL-100 coating, we added $FeCl_3{\cdot}6H_2O$ to a reaction run to investigate the effect of Fe on the selectivity of COL. The result suggested that the addition of Fe^{3+} did not affect the selectivity of COL significantly (Table S2). Additionally, after the MOF coating, the Pt loading decreased (Table S1). As the Pt content may influence the catalytic performance of the supported catalysts, the effects of Pt loading on the hydrogenation were also investigated. Pt/MIL-100 materials with similar Pt contents to the coated samples were used under typical hydrogenation conditions. The reaction results indicated showed no apparent differences in activity and selectivity to COL over the Pt/MIL-100 materials in the range of Pt loadings investigated (Table S2).

Furthermore, hydrogenation using the product COL as the substrate was performed over Pt/MIL-100 and Pt/MIL-100@MIL-100 prepared with four assembly cycles under the investigated conditions. As expected, the rate of C=C bond hydrogenation on the Pt/MIL-100@MIL-100 was clearly slower than that on Pt/MIL-100 (Table S3). Moreover, the hydrogenation rate of COL was slower than that of cinnamaldehyde over Pt/MIL-100@MIL-100. These results indicated that C=C hydrogenation was effectively suppressed over the Pt/MIL-101@MIL-100 catalyst. Based on these results, the remarkably enhanced selectivity of the MIL-100-coated Pt/MIL-100 materials compared with the uncoated materials should be related to both the steric and electron donation effects offered by the MOF shell. Notably, the slight decrease of selectivity to cinnamyl alcohol over the coated sample prepared with six assembly cycles compared to that prepared with four cycles suggested that there is an optimum shell thickness to achieve the highest selectivity because the shell thickness influences the diffusion rate and enrichment of the reactants in the materials.

For the Pt/MIL-100@MIL-100 catalysts, the access of reactants to the fully encapsulated Pt NPs by MIL-100 would be restricted strongly by the microporous windows (≈5.5 and 8.6 Å in size) as well as the aromatic π–π stacking between the phenyl groups of cinnamaldehyde and aryl ligands of MIL-100. As a result of the steric hindrance, cinnamaldehyde diffused into the MOF cavities through the windows most probably with the orientation that the C=O bond pointed inward. Meanwhile, the aromatic π electronic interaction repelled the phenyl group of cinnamaldehyde to the pore wall of MIL-100.[1b] Thus, the terminal C=O bond was able to approach the Pt surface with priority compared to the C=C bond in the middle of the cinnamaldehyde molecule. However, the Pt NPs nestled within the MIL-100 frameworks were surrounded by numerous aryl ligands, which would donate electrons to the Pt surface through the π-bond interaction or coordination (as indicated by the XPS data; Figure 4). A higher electron density of the Pt NPs is more favorable for the activation of the C=O in the cinnamaldehyde.[11] Nevertheless, the MIL-100-coated Pt/MIL-100 materials also showed slightly lower reaction rates than the uncoated Pt/MIL-100 catalyst because of the plausible steric hindrance to the reactants caused by the MIL-100 shell.

It is known that supported metal catalysts can deactivate upon reuse because of the leaching and aggregation of the metal active sites. Therefore, it is crucial that a highly active and selective heterogeneous catalyst is stable and could be reused. In view of this, we performed a recycling experiment and a heterogeneity test on Pt/MIL-100@MIL-100 prepared with four assembly cycles. No appreciable loss in activity and selectivity was observed in the cinnamaldehyde hydrogenation in up to five runs (Figure 6). Subsequently, a heterogeneity test was performed to examine if there was any leaching of active species into the reaction solution. After the removal of the solid catalyst, the reaction solution did not exhibit any further reactivity under similar conditions (Figure S2). Furthermore, the

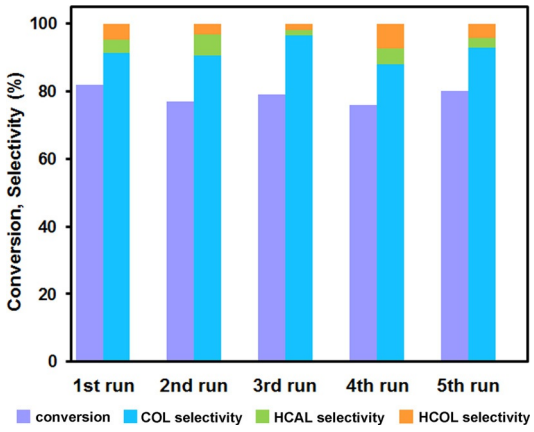

Figure 6. Reuse of the Pt/MIL-100@MIL-100 prepared by four assembly cycles in the hydrogenation of cinnamaldehyde. Reaction conditions: cinnamaldehyde (0.5 mmol), catalyst (Pt 0.2 mol%), isopropyl alcohol (5 mL), 25 °C, 1 atm H_2, 3 h.

solution was analyzed by atomic absorption spectroscopy (AAS), which demonstrated that no metal had leached into the liquid phase during reaction. These findings were in accordance with the results of XRD, N_2 physisorption, and TEM characterization of the reused catalyst. PXRD patterns and TEM images of the reused catalyst were very similar to those of the fresh material (Figure 1, Figure S3), which suggests that both the MOF structure and metal dispersion were mostly preserved after the hydrogenation reaction. Furthermore, the N_2 adsorption isotherm of the recycled catalyst revealed that the porous structure of the catalyst was also maintained (Figure 2, Table S1). These results demonstrated the excellent stability and recyclability of the Pt/MIL-100@MIL-100 catalyst under the investigated conditions, which is believed to be related to the protection effects of the MIL-100 shell to prevent the encapsulated Pt NPs from aggregation and leaching during the reaction.

To demonstrate the general applicability of this MOFs-coating approach to the enhancement of reaction selectivity, we attempted to extend this method to other types of MOFs, for example, NH_2-MIL-101(Al), another representative MOF. This MOF has a rigid zeotype crystal structure and possesses two quasispherical cages (≈2.9 and 3.4 nm) accessible through windows of ≈1.2 and 1.6 nm, respectively. As expected, NH_2-MIL-101(Al) could also be coated successfully onto the Pt/NH_2-MIL-101(Al) surface, and the MOF structure was retained (Figures S4–S6). Furthermore, Pt/NH_2-MIL-101(Al)@NH_2-MIL-101(Al) also exhibited a remarkably enhanced selectivity to cinnamyl alcohol compared to Pt/NH_2-MIL-101(Al) under identical reaction conditions (Figure S7).

Conclusions

We have demonstrated a facile and general strategy for the preparation of new Pt catalysts encapsulated fully in metal–organic frameworks (MOFs) by the coating of MOFs onto the external surface of Pt/MOFs by direct homoepitaxial growth. Such a coating approach can avoid any modification of the core with organic groups to facilitate the formation of the MOF shell over the core. This strategy could also allow the control of the outer MOF shell thicknesses, and the intrinsic properties of the Pt/MOF core were retained. If the obtained Pt/MOFs@MOFs were used as catalysts in the hydrogenation of cinnamaldehyde under atmospheric H_2 pressure and room temperature, the selectivity to the desired cinnamyl alcohol could be enhanced up to 96%, which shows a significant increase compared to that of the uncoated Pt/MOFs (55%). The improved selectivity is believed to be related to the electron donation and confinement effects on the encapsulated Pt nanoparticles offered by the surrounding MOF networks. In addition, the Pt/MOFs@MOFs catalysts were highly stable and reusable, without any metal agglomeration and leaching during a number of recycles. This work might offer a promising new strategy for the synthesis of metal nanocomposites encapsulated fully by MOFs and potentially pave the way to new opportunities for the development of highly selective heterogeneous catalysts.

Experimental Section

Catalyst preparation

All chemicals were purchased from commercial sources and used without further purification. $H_2PtCl_6{\cdot}6H_2O$ (A.R.), $FeCl_3{\cdot}6H_2O$ (A.R.), $AlCl_3{\cdot}6H_2O$ (A.R.), ethanol (A.R.), methanol (A.R.), and isopropyl alcohol (A.R.) were obtained from Sinopharm Chemical Reagent Co., Ltd. 1,4-Benzenedicarboxylic acid (98%), 2-aminoterephthalic acid (99%), PVP (M.W. = 30000), $NaBH_4$ (98%), and cinnamaldehyde (98%) were purchased from Alfa Aesar.

Synthesis of Pt/MIL-100(Fe)

MIL-100(Fe) was synthesized by a solvothermal method reported previously.[8] Pt/MIL-100(Fe) samples were prepared by using a simple colloidal deposition method.[6c] Briefly, the required amount of PVP (PVP monomer/Pt = 10:1, molar ratio) was added to an appropriate volume of H_2PtCl_6 methanol solution (1×10^{-3} M), and the resulting mixture was stirred for 1 h. Then, a freshly prepared methanol solution of $NaBH_4$ (0.1 M, $NaBH_4$/Pt = 5:1, molar ratio) was added rapidly to the mixture under vigorous stirring. After sol formation, which took a few minutes, the activated MIL-100(Fe) was added immediately, and the solution was further stirred for 8 h. Subsequently, the solids were suspended in methanol, stirred for 10 min, and centrifuged. This washing procedure was repeated four times to remove residual Cl^-, Na^+, and PVP as well as Pt species that do not interact with the support. Finally, the sample was dried under vacuum at 100 °C for 2 h to obtain Pt/MIL-100(Fe).

Synthesis of Pt/MIL-100(Fe)@MIL-100(Fe) composites

MIL-100(Fe)-coated Pt/MIL-100(Fe) was prepared according to the following process. Typically, Pt/MIL-100(Fe) (0.1 g) was dispersed in $FeCl_3{\cdot}6H_2O$ ethanol solution (8 mL, 10 mM). The mixture was stirred for 1 h at RT. Subsequently, benzenetricarboxylic acid ethanol solution (8 mL, 10 mM) was added, and the resulting mixture was stirred for 30 min at 70 °C. The MIL-100(Fe)-coated Pt/MIL-100(Fe) composite was collected by centrifugation and washed with ethanol. After the required number of cycles, the sample was washed thoroughly with ethanol and dried under vacuum at 100 °C. AAS indicated that the ratio of the leached Pt to the loading on Pt/MIL-100 was below 1.0% after MOF coating, which indicates that the leaching of Pt during the coating was not significant.

Synthesis of Pt/NH_2-MIL-101(Al)@NH_2-MIL-101(Al) composites

NH_2-MIL-101(Al) was synthesized by a solvothermal method reported previously.[12] Pt/NH_2-MIL-101(Al) was prepared by using the same procedure as described above for the synthesis of Pt/MIL-100(Fe). NH_2-MIL-101(Al)-coated Pt/NH_2-MIL-101(Al) was prepared according to the following process. Typically, Pt/NH_2-MIL-101(Al) (0.1 g) was dispersed in $AlCl_3{\cdot}6H_2O$ ethanol solution (8 mL, 10 mM). The mixture was stirred for 1 h at RT. Subsequently, 2-aminoterephthalic acid methanol solution (8 mL, 10 mM) was added, and the resulting mixture was stirred for 30 min at 70 °C. The NH_2-MIL-101(Al)-coated composite was collected by centrifugation and washed with ethanol. After the required number of cycles, the sample was washed thoroughly with ethanol and dried under vacuum at 100 °C.

Catalyst characterization

PXRD patterns of the samples were obtained by using a Rigaku diffractometer (D/MAX-IIIA, 3 kW) that employed CuK_α radiation ($\lambda =$ 0.1543 nm) at 40 kV and 40 mA at RT.

Low-temperature N_2 adsorption–desorption isotherms were measured at 77 K by using a Micromeritics ASAP 2020 instrument. The sample was evacuated at 150 °C for 12 h before the analysis. The metal contents of the samples were determined quantitatively by AAS by using a HITACHI Z-2300 instrument.

The morphologies of the samples were characterized by TEM (JEOL, JEM-2010HR) operated at 200 kV. XPS measurements were performed by using a Kratos AxisUltra DLD system with a base pressure of 10^{-9} torr. Binding energies were referenced to the C 1s line at 284.6 eV from adventitious carbon.

Catalytic reactions

General procedure for the hydrogenation of cinnamaldehyde

Typically, cinnamaldehyde (0.5 mmol) and an appropriate amount of catalyst (Pt 0.2 mol%) were added to isopropyl alcohol (5 mL). The reaction mixture was stirred at RT under 1 atm hydrogen atmosphere. After reaction for the desired time, the solid was isolated from the solution by centrifugation and washed with isopropyl alcohol. The liquid phase was subsequently analyzed by GC–MS (Shimadzu GCMSQP5050A equipped with a 0.25 mm × 30 m DB-WAX capillary column).

Recyclability of the Pt/MIL-100(Fe)@MIL-100(Fe) catalyst

For the recyclability test, the reactions were performed under the same reaction conditions as described above except with the use of the recovered catalyst. At the end of catalytic reaction, the solid was recovered from the reaction mixture by centrifugation, washed with isopropyl alcohol, and then heated at 100 °C under vacuum.

Acknowledgements

This work was supported by the National Natural Science Foundation of China (21322606, 21436005, 21406075, and 21576095), the Fundamental Research Funds for the Central Universities (2014ZB0004, 2015ZP002, and 2015PT004), Guangdong Natural Science Foundation (2013B090500027), and China Postdoctoral Science Foundation (2014M550437, 2015T80908).

Keywords: heterogeneous catalysis · hydrogenation · metal–organic frameworks · nanoparticles · platinum

[1] a) K. P. de Jong, *Synthesis of Solid Catalysts*, Wiley-VCH, Weinheim, **2009**; b) K. R. Kahsar, D. K. Schwartz, J. W. Medlin, *J. Am. Chem. Soc.* **2014**, *136*, 520 – 526.

[2] a) Q. Zhang, I. Lee, J. B. Joo, F. Zaera, Y. Yin, *Acc. Chem. Res.* **2013**, *46*, 1816 – 1824; b) I. Lee, M. A. Albiter, Q. Zhang, J. Ge, Y. Yin, F. Zaera, *Phys. Chem. Chem. Phys.* **2011**, *13*, 2449 – 2456; c) Y. Zhang, B. Y. W. Hsu, C. Ren, X. Li, J. Wang, *Chem. Soc. Rev.* **2015**, *44*, 315 – 335; d) S. Liu, M.-Y. Han, *Chem. Asian J.* **2010**, *5*, 36 – 45; e) S. H. A. M. Leenders, R. Gramage-Doria, B. de Bruin, J. N. H. Reek, *Chem. Soc. Rev.* **2015**, *44*, 433 – 448; f) Y. Liu, Z. Tang, *Adv. Mater.* **2013**, *25*, 5819 – 5825; g) Y. Zhang, S. N. Riduan, *Chem. Soc. Rev.* **2012**, *41*, 2083 – 2094.

[3] a) V. Pascanu, A. B. Gómez, C. Ayats, A. E. Platero-Prats, F. Carson, J. Su, Q. Yao, M. À. Pericàs, X. Zou, B. Martín-Matute, *ACS Catal.* **2015**, *5*, 472 – 479; b) S. Goel, S. I. Zones, E. Iglesia, *J. Am. Chem. Soc.* **2014**, *136*, 15280 – 15290; c) J. Liu, S. Qiao, S. B. Hartono, G. Lu, *Angew. Chem. Int. Ed.* **2010**, *49*, 4981 – 4985; *Angew. Chem.* **2010**, *122*, 5101 – 5105; d) M. Zhang, K. Fang, M. Lin, B. Hou, L. Zhong, Y. Zhu, W. Wei, Y. Sun, *J. Phys. Chem. C* **2013**, *117*, 21529 – 21538.

[4] a) M. Li, D. Li, M. O'Keeffe, O. M. Yaghi, *Chem. Rev.* **2014**, *114*, 1343 – 1370; b) Z. Hu, B. J. Deibert, J. Li, *Chem. Soc. Rev.* **2014**, *43*, 5815 – 5840.

[5] a) A. Aijaz, Q. Xu, *J. Phys. Chem. Lett.* **2014**, *5*, 1400 – 1411; b) H. R. Moon, D.-W. Lim, M. P. Suh, *Chem. Soc. Rev.* **2013**, *42*, 1807 – 1824; c) G. Férey, C. Mellot-Draznieks, C. Serre, F. Millange, J. Dutour, S. Surblé, I. Margiolaki, *Science* **2005**, *309*, 2040 – 2042; d) H. Furukawa, N. Ko, Y. B. Go, N. Aratani, S. B. Choi, E. Choi, A. Ö. Yazaydin, R. Q. Snurr, M. O'Keeffe, J. Kim, O. M. Yaghi, *Science* **2010**, *329*, 424 – 428.

[6] a) A. Dhakshinamoorthy, H. Garcia, *Chem. Soc. Rev.* **2012**, *41*, 5262 – 5284; b) L. Chen, H. Chen, R. Luque, Y. Li, *Chem. Sci.* **2014**, *5*, 3708 – 3714; c) H. Liu, Y. Liu, Y. Li, Z. Tang, H. Jiang, *J. Phys. Chem. C* **2010**, *114*, 13362 – 13369; d) R. J. T. Houk, B. W. Jacobs, F. E. Gabaly, N. N. Chang, A. A. Talin, D. D. Graham, S. D. House, I. M. Robertson, M. D. Allendorf, *Nano Lett.* **2009**, *9*, 3413 – 3418; e) L. B. Vilhelmsen, K. S. Walton, D. S. Sholl, *J. Am. Chem. Soc.* **2012**, *134*, 12807 – 12816.

[7] a) G. Lu, S. Li, Z. Guo, O. K. Farha, B. G. Hauser, X. Qi, Y. Wang, X. Wang, S. Han, X. Liu, J. S. DuChene, H. Zhang, Q. Zhang, X. Chen, J. Ma, S. C. J. Loo, W. D. Wei, Y. Yang, J. T. Hupp, F. Huo, *Nat. Chem.* **2012**, *4*, 310 – 316; b) L. He, Y. Liu, J. Liu, Y. Xiong, J. Zheng, Y. Liu, Z. Tang, *Angew. Chem. Int. Ed.* **2013**, *52*, 3741 – 3745; *Angew. Chem.* **2013**, *125*, 3829 – 3833; c) K. Na, K. M. Choi, O. M. Yaghi, G. A. Somorjai, *Nano Lett.* **2014**, *14*, 5979 – 5983; d) D. Esken, S. Turner, O. I. Lebedev, G. V. Tendeloo, R. A. Fischer, *Chem. Mater.* **2010**, *22*, 6393 – 6401; e) J. Hermannsdörfer, M. Friedrich, N. Miyajima, R. Q. Albuquerque, S. Kümmel, R. Kempe, *Angew. Chem. Int. Ed.* **2012**, *51*, 11473 – 11477; *Angew. Chem.* **2012**, *124*, 11640 – 11644; f) H. Liu, Y. Li, R. Luque, H. Jiang, *Adv. Synth. Catal.* **2011**, *353*, 3107 – 3113; g) T. Ishida, M. Nagaoka, T. Akita, M. Haruta, *Chem. Eur. J.* **2008**, *14*, 8456 – 8460; h) Z. Guo, C. Xiao, R. V. Maligal-Ganesh, L. Zhou, T. W. Goh, X. Li, D. Tesfagaber, A. Thiel, W. Huang, *ACS Catal.* **2014**, *4*, 1340 – 1348; i) C. Wang, Q. Gong, Y. Zhao, J. Li, A. D. Lueking, *J. Catal.* **2014**, *318*, 128 – 142; j) Y. Huang, S. Liu, Z. Lin, W. Li, X. Li, R. Cao, *J. Catal.* **2012**, *292*, 111 – 117; k) J. Long, H. Liu, S. Wu, S. Liao, Y. Li, *ACS Catal.* **2013**, *3*, 647 – 654.

[8] P. Horcajada, S. Surblé, C. Serre, D.-Y. Hong, Y.-K. Seo, J.-S. Chang, J.-M. Grenèche, I. Margiolaki, G. Férey, *Chem. Commun.* **2007**, 2820 – 2822.

[9] a) L. A. Saudan, *Acc. Chem. Res.* **2007**, *40*, 1309 – 1319; b) P. Dupau in *Organometallics as Catalysts in the Fine Chemical Industry* (Eds.: M. Beller, H.-U. Blaser), Springer, Heidelberg, **2012**; c) G. Kennedy, L. R. Baker, G. A. Somorjai, *Angew. Chem. Int. Ed.* **2014**, *53*, 3405 – 3408; *Angew. Chem.* **2014**, *126*, 3473 – 3476; d) K. Q. Sun, Y. C. Hong, G. R. Zhang, B. Q. Xu, *ACS Catal.* **2011**, *1*, 1336 – 1346.

[10] a) A. Giroir-Fendler, D. Richard, P. Gallezot, *Catal. Lett.* **1990**, *5*, 175 – 182; b) A. Giroir-Fendler, D. Richard, P. Gallezot, *Faraday Discuss.* **1991**, *92*, 69 – 77; c) M. S. Ide, B. Hao, M. Neurock, R. J. Davis, *ACS Catal.* **2012**, *2*, 671 – 683.

[11] a) C.-Y. Hsu, T.-C. Chiu, M.-H. Shih, W.-J. Tsai, W.-Y. Chen, C.-H. Lin, *J. Phys. Chem. C* **2010**, *114*, 4502 – 4510; b) J. Haubrich, D. Loffreda, F. Delbecq, P. Sautet, Y. Jugnet, C. Becker, K. Wandelt, *J. Phys. Chem. C* **2010**, *114*, 1073 – 1084; c) S. C. Tsang, N. Cailuo, W. Oduro, A. T. S. Kong, L. Clifton, K. M. K. Yu, B. Thiebaut, J. Cookson, P. Bishop, *ACS Nano* **2008**, *2*, 2547 – 2553.

[12] M. Hartmann, M. Fischer, *Microporous Mesoporous Mater.* **2012**, *164*, 38 – 43.

Received: November 15, 2015
Revised: December 15, 2015
Published online on January 25, 2016